PAPER • OPEN ACCESS

Detection of carbon monoxide using a polarization-multiplexed erbium dual-comb fiber laser

Journal of Physics: Photonics

OPEN ACCESS

RECEIVED
16 July 2024

REVISED
9 September 2024

ACCEPTED FOR PUBLICATION
29 September 2024

PUBLISHED
10 October 2024

PAPER

Detection of carbon monoxide using a polarization-multiplexed erbium dual-comb fiber laser

P E Collin Aldia[1,2,*], **Jiayang Chen**[1,3], **Jonas K C Ballentin**[1], **Lukas W Perner**[4,5] and **O H Heckl**[1]

[1] Optical Metrology Group, Faculty of Physics, University of Vienna, Boltzmanngasse 5, 1090 Vienna, Austria
[2] Vienna Doctoral School in Physics, University of Vienna, Boltzmanngasse 5, 1090 Vienna, Austria
[3] State Key Laboratory of Precision Measurement Technology and Instruments, Department of Precision Instrument, Tsinghua University, Beijing 100084, People's Republic of China
[4] Christian Doppler Laboratory for Mid-IR Spectroscopy and Semiconductor Optics, Faculty Center for Nano Structure Research, Faculty of Physics, University of Vienna, Boltzmanngasse 5, 1090 Vienna, Austria
[5] Currently at the Laboratoire Temps-Fréquence, Institut de Physique, Université de Neuchâtel.
[*] Author to whom any correspondence should be addressed.

E-mail: collinaldia@univie.ac.at and oliver.heckl@univie.ac.at

Keywords: dual-comb lasers, fiber lasers, dual-comb spectroscopy, optical frequency combs

Abstract

We present a simple method to develop a compact, reliable, and robust free-running erbium single-cavity dual-comb (DC) laser via polarization multiplexing. The key features of our design include dynamic tuning in the difference in repetition rates of the laser, long-term stability, and the use of off-the-shelf components. Polarization multiplexing exploits the fast and slow axes of the fiber, while modelocking is achieved through a nonlinear amplifying loop mirror scheme using readily available components. The laser operates at a repetition rate of around 74.74 MHz with a tuning capability in the difference in repetition rates from 500 Hz to 200 kHz. This tunability makes the system more flexible for DC spectroscopy experiments. Consequently, using this laser, we demonstrated a proof-of-principle DC spectroscopy of carbon monoxide, operating without any active stabilization.

1. Introduction

Optical Frequency Combs (OFCs) have become ubiquitous tools in various fields, among them molecular fingerprinting [1], trace gas sensing [2], precision ranging [3], atomic clocks [4], and high-harmonic generation [5]. In particular, owing to their high coherence, high-frequency resolution, and broadband spectra, OFCs are considered to be an ideal tool/light source for molecular spectroscopy [6–8]. This technique, called direct frequency comb spectroscopy, has enabled groundbreaking results in fields as diverse as time-resolved spectroscopy [9, 10], human breath analysis [11], and real-time sensing [12]. Conventionally, Fourier transform spectrometers [13, 14], grating-based spectrometers, and virtually imaged phase arrays [15] are used as spectrometers. However, these systems require bulky setups, long scanning ranges, and rigorous alignment.

In contrast, so-called dual-comb (DC) systems eliminate all the aforementioned problems of conventional spectrometers. DC spectroscopy combines the advantages of the above-mentioned single-comb techniques by leveraging the properties of OFCs. In essence, a DC system consists of two mutually coherent modelocked lasers with spectral overlap with slightly different pulse repetition rates. In the frequency domain, this results in two frequency combs with slightly different comb line spacing. The optical beating between the comb lines of these two OFCs generates a down-converted radio frequency (RF) signal. Conveniently, only a fast photodiode is necessary to detect this resulting RF beat signal, making the above-mentioned complex spectrometer assemblies unnecessary. This RF interferogram contains relevant spectral information in the optical domain. Thus, high-resolution spectra can be obtained at an acquisition rate considerably higher than that of single-comb spectroscopy (mostly limited by the difference in repetition rates of the two combs) without the need for any sophisticated measurement tools. This technique was first

proposed by Schiller [16], and later demonstrated by Coddington *et al* [7, 17]. Thereafter, DC systems have found a wide range of applications, notably in ranging [18, 19], absorption spectroscopy [20] and CARS [9, 21]. Since the two combs have to be mutually coherent (i.e. retain a stable relation between Comb1 and Comb2), they need to be stabilized to each other. This effectively shifts the complexity of the detection apparatus to the laser source, again leading to complicated setups. Several ways to overcome this challenge were proposed, among them, phase locking the two combs to an external cavity diode laser [17, 22] or using adaptive sampling techniques [23, 24]. An elegant solution is so-called single-cavity DC (SCDC) lasers, where both combs are generated in a single laser cavity. This guarantees good mutual coherence due to common-mode noise cancellation. Consequently, applications without comb-mode resolution do not require active stabilization. Since the advent of SCDC, several schemes have been contrived, among them bi-directional splitting [25, 26], branched optical paths in a birefringent crystal [27, 28], spatial separation [29], polarization multiplexing [30, 31], or spectral subdivision, commonly called dual-color systems [32–35].

All of the SCDC systems mentioned above are based on modelocked lasers. Particularly, OFCs based on polarization maintaining (PM) fibers modelocked via nonlinear amplifying loop mirror (NALM) are known to be more robust and reliable, also offering extremely low free-running noise properties when operated in certain regimes [36–38]. Since the first demonstration by Kuse *et al* [37], the NALM modelocking scheme has become one of the standard tools. The NALM scheme utilizes the superposition of two counter-propagating waves. The nonlinear phase shift accumulated in each direction is intensity-dependent. Therefore, constructive interference is sustained within the cavity, while destructive interference is rejected. This resembles an artificial saturable absorber and is the basis for modelocking our laser. Fellinger *et al* [32] and Nakajima *et al* [39] demonstrated DC systems based on PM fibers modelocked using a NALM. The former is a dual-color system based on spectral subdivision while the latter exploits mechanical sharing of components. In the former setup, additional spectral broadening is required to overlap the dual-color laser and obtain an RF beat signal. Other approaches include polarization multiplexing to develop a DC system using a NALM modelocking scheme [40, 41]. More recently, Iwakuni *et al* [42] studied the noise properties of an SCDC modelocked using a NALM based on polarization multiplexing with gain sharing. They reported a low phase noise (PN) for their system, making it a suitable candidate for DC spectroscopy. This type of DC system with polarization splitting has inherent spectral overlap, making spectral broadening unnecessary.

In this work, we combine the NALM modelocking scheme and the features of a PM fiber to develop a compact, robust, and reliable SCDC laser. A PM fiber-based polarizing beam splitter (PBS) is utilized to split the polarization of the light within the cavity to generate the dual comb. In free-running DC operation (i.e. without any active stabilization), the difference in repetition rates between the two combs Δf_{rep} was tuned over almost three orders of magnitude, from 500 Hz to 200 kHz while maintaining stable DC operation. This tuning possibility gives us a convenient handle on the acquisition rate, which directly depends on the difference in repetition rates Δf_{rep} and the non-aliasing bandwidth $\Delta\nu$. The latter is the maximum allowed overlap between the two combs before spectral aliasing occurs. It is given by [43]

$$\Delta\nu \leqslant \frac{f_{\mathrm{rep},1}^2}{2\Delta f_{\mathrm{rep}}}. \tag{1}$$

$f_{\mathrm{rep},1}$ is the repetition rate of one of the combs. With the possibility to tune Δf_{rep} between 500 Hz–200 kHz, we were able to achieve a non-aliasing bandwidth of 0.014–5.59 THz (0.12–45.93 nm at 1570 nm). While modelocking could be maintained over the whole tuning range, we chose a Δf_{rep} of 1.04 kHz for our proof-of-principle DC spectroscopy demonstration, resulting in a $\Delta\nu$ of 2.69 THz at 1570 nm. This value of the difference in repetition rates is an optimal compromise between a fast acquisition rate and large non-aliasing bandwidth for our target application. Our system is, thus, based on the aforementioned NALM technique and polarization multiplexing, has inherent spectral overlap, and is compact and robust without active stabilization, making it an ideal basis for field-deployable spectroscopy.

2. Experimental setup

As shown in figure 1(a), the Erbium (Er) SCDC laser setup consists of an all-PM-fiber section and two free-space sections. The fiber section comprises a PM wavelength division multiplexer (WDM), an Er-doped gain fiber (Liekki Er80-4/125-HD-PM) with a length of 78 cm, two PBSs, and two birefringent polarizing beam combiner collimators (PBCC). Since Er-doped gain fibers have less gain compared to ytterbium-doped gain fibers, two 980 nm pump diodes (3SP 3CN01800JL) are used for initiating DC operation. The pump light is combined at a PBC which then travels through the common port of the WDM to the gain fiber. The light exiting the PBCC travels through various polarization optics in the free-space section.

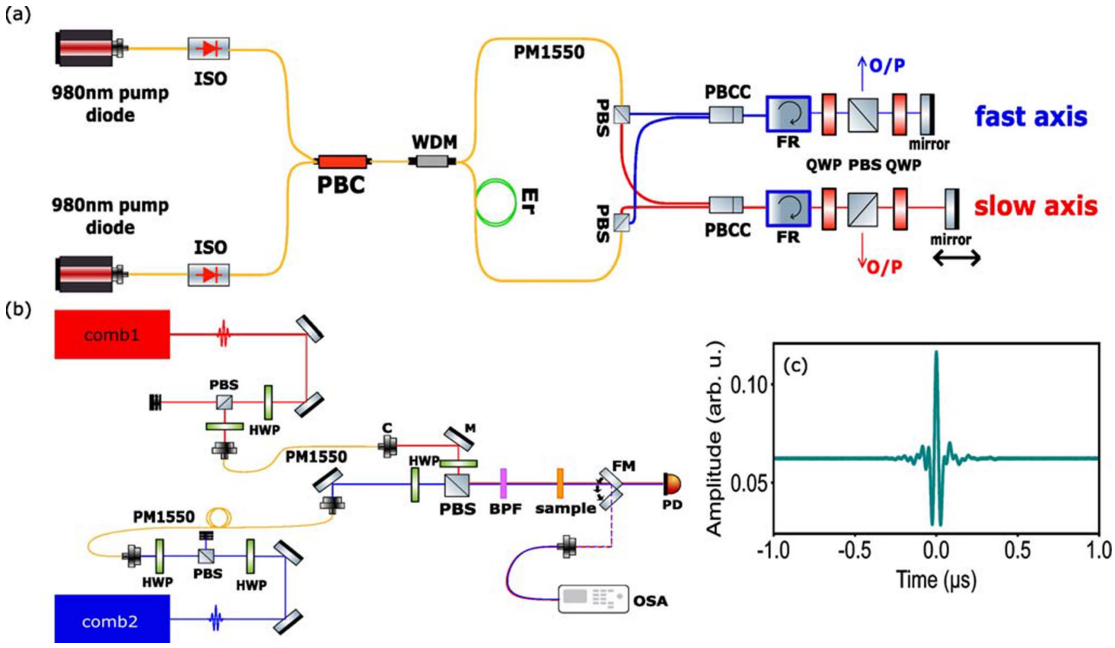

Figure 1. (a) The Er DC laser setup. ISO: isolator; PBC: polarizing beam combiner; WDM: wavelength division multiplexer; Er: Er-doped gain fiber; PBS: polarizing beam splitter; PBCC: polarizing beam combiner collimator; FR: Faraday rotator; QWP: quarter-waveplate. (b) Experimental setup to obtain the optical beating between the two combs. HWP: half-waveplate; BPF: bandpass filter; C: collimator; M: mirror; FM: flip mirror; PD: photodiode; OSA: Optical Spectrum Analyzer. (c) A single-shot interferogram recorded using the setup in (b).

The modelocking scheme used here is similar to [36]. The polarization of light in the fiber ring is split at the fiber-PBS into the fast and slow axes of the PM fiber. It is at this fiber component where polarization multiplexing of DC operation begins. After the splitting, the light exits the respective PBCCs into the free-space arms. The two combs are individually modelocked in their respective arms. The non-reciprocal phase bias introduced by the Faraday rotator and the quarter-waveplate, along with the free-space PBS and the other quarter-waveplate initiate modelocking the laser.

The two combs share the gain medium and also 116 cm of single-mode PM1550 fiber. The unshared fiber paths have a length of 48.4 cm and 48.75 cm for slow and fast axes, respectively. The linear free-space arms have virtually identical lengths around 13.5 cm. Additionally, one of the end mirrors is mounted on a translational stage to fine-tune the difference in repetition rates Δf_{rep}. To start the DC operation, we first tune the waveplate positions for each arm individually (i.e. with the other arm blocked) to obtain self-starting states. Once these states have been found, we increase the pump currents to the sum of the pump currents required for modelocking each comb individually. At this value of pump current, we adjust the linear losses in the two arms by rotating the quarter-waveplate between the PBS and the end mirror. The DC operation can be initiated by ensuring that linear losses in the two arms are comparable. Afterward, we gradually decrease the pump current until the single-pulse operation is achieved for both combs. At this point, only one of the pump diodes is required to maintain the DC state. We ensure single-mode operation by verifying the absence of multiple interferograms on an oscilloscope trace spanning $\Delta t = 1/\Delta f_{\mathrm{rep}}$. Once this is achieved, the system stays in DC operation for several months.

3. DC characterization

Our polarization-multiplexed Er SCDC laser has a nominal repetition rate f_{rep} around 74.74 MHz with a difference in repetition rates Δf_{rep} tunable from 500 Hz to 200 kHz. As shown in figure 2(a), the output spectra from the two combs are extremely similar as expected for a DC system based on polarization multiplexing. The spectra are centered around 1571.8 nm and 1564.6 nm with a full width at half maximum (FWHM) of 20.09 nm and 23.55 nm for fast and slow axes, respectively. We attribute the discrepancy in center wavelength to a difference in linear losses among the two arms [44]. The net dispersion of the cavity is calculated to be ~ -0.015 ps^2 at their center wavelengths. The pulse duration of the two combs was measured using an in-house developed autocorrelator and found to be around 240 fs. The RF spectrum of the respective pulse trains is measured using a fast photodiode (Thorlabs DET08CL/M) as shown in figures 2(c) and (d). The higher harmonics can also be seen in these plots and the absence of side peaks around the main

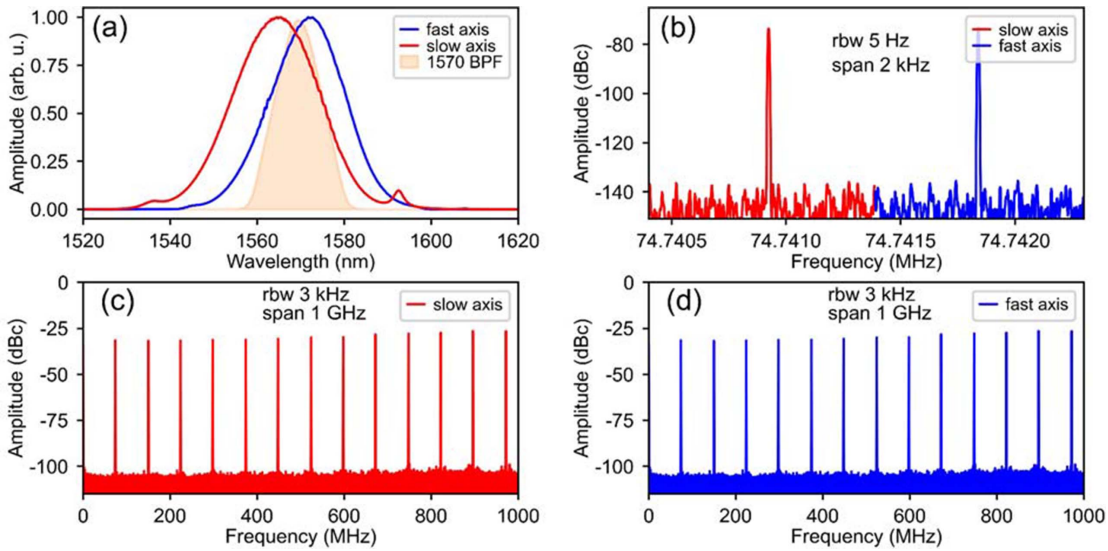

Figure 2. (a) Output spectra of the two combs measured using an optical spectrum analyzer (Yokogawa AQ6374). The shaded region shows the transmission curve of the bandpass filter. (b) The RF spectrum of the laser was measured using a fast photodiode. This plot shows a single measurement and the two colors are just a guide for visual representation. (c) and (d) 1 GHz span and a resolution bandwidth (rbw) of 3 kHz of the individual combs showing their repetition rates and higher harmonics for fast and slow axes, respectively. All the RF spectra were recorded using an RF spectrum analyzer (Keysight PXA N9030B).

peaks confirms the clean single-pulse operation. In this state, the output power from the laser was directly measured to be 14 mW and 11 mW for fast and slow axes, respectively. To determine the repetition rates of the laser, $f_{\mathrm{rep},1}$ and $f_{\mathrm{rep},2}$, and the difference in repetition rates Δf_{rep}, the output from the two arms are sent to a Thorlabs PDA05CF2 photodiode (figure 2(b)).

To record the beat signal (the interferogram as shown in figure 1(c)), the two combs are spatially overlapped, and the signal is measured using a simple photodiode (Thorlabs PDA05CF2) (figure 1(b)). Several other steps were also contrived to ensure coherent beating between the two combs. Apart from the spatial overlap, the polarization state of the two combs is monitored via various polarization optics. An optical bandpass filter is inserted to cut the overlapped region of the two spectra (figure 1(b)). A 48 MHz low-pass filter is used to remove the repetition rates of the laser $f_{\mathrm{rep},1}$ and $f_{\mathrm{rep},2}$ before the signal is recorded on an oscilloscope (LeCroy WavePro 760Zi). Calculating the Fast-Fourier-Transform (FFT) of this interferogram yields the down-converted RF spectrum. The center frequency of this down-converted RF spectrum is associated with the difference in the carrier-envelope offset (CEO) frequency. However, this parameter is not easy to access, and it is, therefore, difficult to shift the down-converted spectrum in the RF domain deliberately. This effectively limits the extent to which the full non-aliasing bandwidth can be used for spectroscopy experiments. Nevertheless, the non-aliasing bandwidth was large enough for this work with our specified laser parameters. As this paper is focused on the capabilities of the system in free-running operation, controlling the CEO frequency (as well as dispersion tuning) is left to future investigation.

3.1. Intra-cavity cross-talk and resolution

When two pulse trains travel within the same cavity or share some parts of the cavity, they interact with each other [45]. This causes the formation of spurious signals in the time traces. As seen in the work of Fellinger *et al* [32], a simple delay line in one of the arms conveniently shifts these spurious signals with respect to the interferogram before the spatial overlap of the two combs. It is to be noted that the overall performance of the system does not degrade with the introduction of the extra path. Thus, by creating an appropriate extra-cavity path length between the two arms, we can achieve an undisturbed time window around the center burst. This is relevant for DC spectroscopy since the resolution in the RF domain directly corresponds to the inverse of the measured time window. For 1 m of fiber inserted into one of the arms delays the spurious signal by ~200 μs (figure 3(a)). This would correspond to an undisturbed time window of 400 μs around the center burst. For a nominal repetition rate f_{rep} around 74.74 MHz and the difference in repetition rates Δf_{rep} of 1.04 kHz, this time window would accord to an optical resolution ~180 MHz (a resolution of 0.001 nm at 1570 nm).

3.2. Non-aliasing bandwidth

As mentioned in section 1, the non-aliasing bandwidth $\Delta\nu$ (equation (1)) is an important parameter, as it gives the maximal allowed spectral overlap. Therefore, once the two arms are spatially overlapped, we insert a

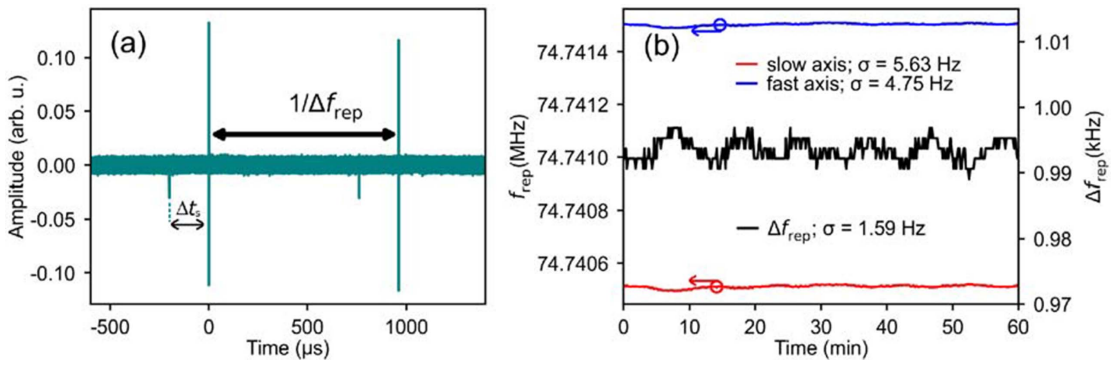

Figure 3. (a) Time trace recorded on an oscilloscope (LeCroy WavePro 760Zi) where the center-bursts are separated in time $\Delta t = 1/\Delta f_{rep}$. The spurious signals resulting from the intracavity pulse collisions are visible as small side-peaks (discussed in section 3.1). (b) The drift of the repetition rates f_{rep} and their difference Δf_{rep}.

bandpass filter with a FWHM of 12 nm to avoid aliasing. For the above laser parameters, the non-aliasing bandwidth is calculated to be 22.13 nm at 1570 nm. Since the non-aliasing bandwidth depends on the repetition rates of the laser f_{rep} and the difference in repetition rates Δf_{rep}, we investigated the tuning possibility in Δf_{rep}. We were able to tune the Δf_{rep} from 500 Hz to 200 kHz, above which we observed a reduction of non-aliasing bandwidth and mutual coherence. We effectively tuned the Δf_{rep} for the above range without losing DC operation. First, we tuned to higher values of Δf_{rep} and then gradually decreased to small values. Reducing the lower bound will compromise the maintenance of DC operation due to injection locking, and therefore, we lost mode-locking in one of the combs for Δf_{rep} slightly below 500 Hz. Nonetheless, a stable DC operation was maintained for Δf_{rep} higher than 200 kHz. Even though a Δf_{rep} of 500 Hz would give a large value of $\Delta\nu$, the long-term stability of the laser was compromised. However, Δf_{rep} of around 1 kHz ensured better performance in terms of stability over several months and also a reasonable value of $\Delta\nu$. Depending on the applications, one could tune the value of Δf_{rep}, compromising the acquisition rate or the non-aliasing bandwidth. For comb-mode resolved DC systems, the spectral resolution is only determined by the repetition rate of the laser f_{rep} and not Δf_{rep}. However, for other cases (apodized interferograms), a higher value of Δf_{rep} and a lower value of f_{rep} result in a higher resolution.

3.3. Frequency stability

The frequency stability of this DC system was measured in free-running operation without any active stabilization. To carry out this measurement, we observed the drifts of the two individual repetition rates for one hour (figure 3(b)). However, the drift in Δf_{rep} was calculated by the difference of $f_{rep,1}$ and $f_{rep,2}$, and not measured directly (figure 3(b); black line). The value of Δf_{rep} for this measurement was set close to 1 kHz. The drift in the magnitude of the individual repetition rates was estimated by calculating the standard deviation σ, which was computed to be 5.63 Hz and 4.75 Hz for slow and fast axes, respectively. However, the measured drift in Δf_{rep} shows a reduction by a factor of three with $\sigma = 1.59$ Hz. This value can be further reduced by improving the mechanical stability of the laser or proper boxing of the system. However, it is to be noted that an accurate frequency measurement using a free-running DC system is not possible. Even though Δf_{rep} is passively stabilized, the variations in individual repetition rates can introduce uncertainty to the measurement results. Nevertheless, the value of the drift was already good enough to carry out proof-of-principle measurements with this DC system.

3.4. Relative intensity noise (RIN) and PN

The RIN and the PN of the DC system in free-running operation were measured using a Rohde & Schwarz FSWP8 PN Analyzer (PNA). For the RIN measurements, we used a 20.6 MHz bandwidth (BW) Thorlabs DET05D2 biased InGaAs detector, while for PN, a 5 GHz BW Thorlabs DET08CL InGaAs fast photodiode, in combination with the PNA. However, in the case of PN measurements, the noise at the 46th harmonic was measured to increase measurement sensitivity with respect to the shot-noise limit. The measured value is then corrected to obtain the PN at the repetition rate of the laser (first harmonic). Therefore, an additional low-noise amplifier (Mini-Circuits ZX60-63GLN) was inserted, which did not add any measurable noise to the system but only amplified the RF signal to achieve a stronger carrier power.

The RIN measurement of the system in DC operation is depicted in figure 4(a). The technical noise below 1 kHz can be suppressed further by improving the mechanical stability of the system. The equidistant peaks that are visible in both cases starting from ~1 kHz are the difference in repetition rates of the laser and

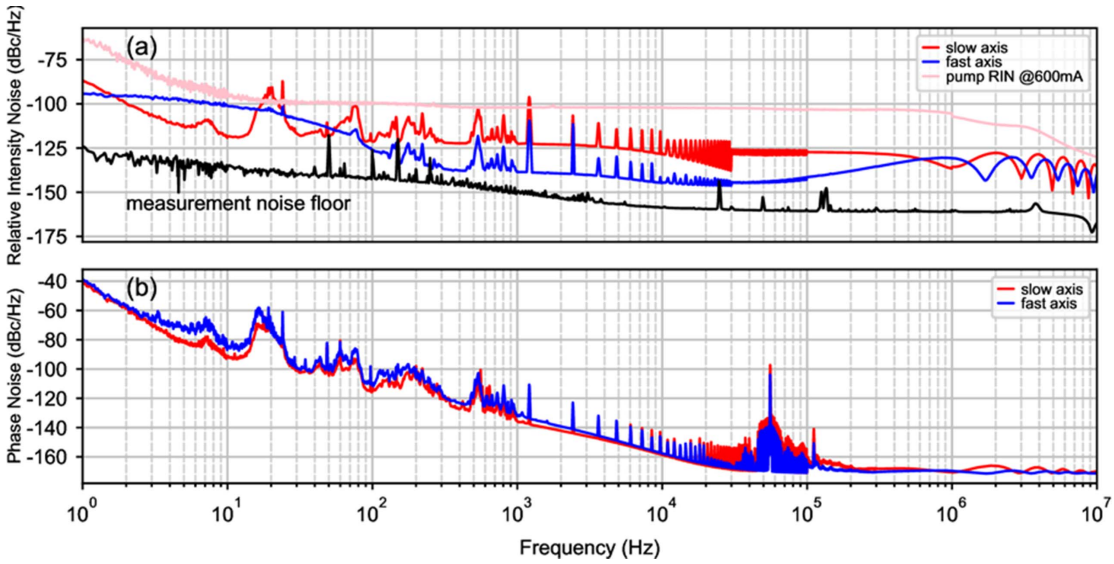

Figure 4. (a) RIN measurements of both slow (red) and fast (blue) axes measured at 600 mA in DC operation. The pump RIN at the same pump current is depicted as well. (b) PN measurements of the two combs measured at the 46th harmonic and re-normalized to the first harmonic (f_{rep}) in DC operation.

its harmonics. For DC systems where the two combs share the common cavity and the gain fiber, such peaks can be visible [32]. The amplitude change of the oscillations at 30 kHz and 100 kHz is due to the continuous averaging of the PNA and not a change in the RIN of the system. Each averaging segment of the PNA has different integration values, which then leads to a change in the amplitude at these intervals. The root-mean-square (RMS) integrated RIN from 1 Hz–1 MHz was calculated to be 0.054 % and 0.053 % for fast and slow axes, respectively. However, for the range 10 Hz – 100 kHz, it is 0.007 % and 0.01 %, respectively. This value of RMS RIN is comparable to the single-comb operation of NALM-based fiber lasers [36]. On the other hand, the PN of the first harmonic for both the fast and slow axes is plotted in figure 4(b). Similar to the RIN, technical noise and the difference in repetition rates Δf_{rep} and its harmonics are visible for frequencies lower and greater than 1 kHz, respectively. The integrated timing jitter for the two arms in the frequency range from 10 Hz to 1 MHz was calculated to be 4700 fs and 2300 fs for fast and slow axes, respectively. The measurement discrepancies can be attributed to the low-frequency region caused by the heavy construction site next door. Therefore, measurements carried out in succession can have different environmental conditions. Nevertheless, compared to previously reported PN of fiber-based SCDC system, our laser outperforms throughout the whole frequency range [42], while it is on par with solid-state SCDC system [46].

For spectroscopic experiments, the RIN and PN can contribute to the quality of the interferograms and the down-converted RF spectrum. The frequencies that will be of importance are directly linked to the time window of acquisition. For instance, a 20 μs time window means that the RIN and PN for all the frequencies above 50 kHz will become relevant. In the frequency domain, both RIN and PN contribute to linewidth broadening; however, it is negligible in our case with a rudimentary calculation of β-separation line [47]. Nevertheless, in the time domain, only PN contributes to the signal-to-noise ratio (SNR) of the resulting interferogram after coherent averaging. When the timing jitter of the two combs is relatively the same, one comb will sample the other comb at the same point. This will result in interferograms with data points sampled at the same position. Therefore, many interferograms can be averaged, resulting in better data processing and high SNR. Moreover, the PN of both the combs is very similar in performance, which is crucial for DC spectroscopic applications, as shown in the next section.

4. DC spectroscopy of carbon monoxide ($^{12}C^{16}O$)

In this section, we demonstrate a proof-of-principle DC spectroscopy experiment of a carbon monoxide (CO) reference cell at ambient temperature. To the best of our knowledge, DC spectroscopic capabilities have never been demonstrated before for such a laser design at this wavelength. The absorption features of the gas are measured at a pressure of 790 Torr with an effective path length of 30 cm. For these measurements, a time window of 20 μs was set, and 250 interferograms were recorded in sequence using an oscilloscope (LeCroy WavePro 760Zi). This time window corresponds to an optical frequency resolution of 3.6 GHz for $\Delta f_{rep} =$

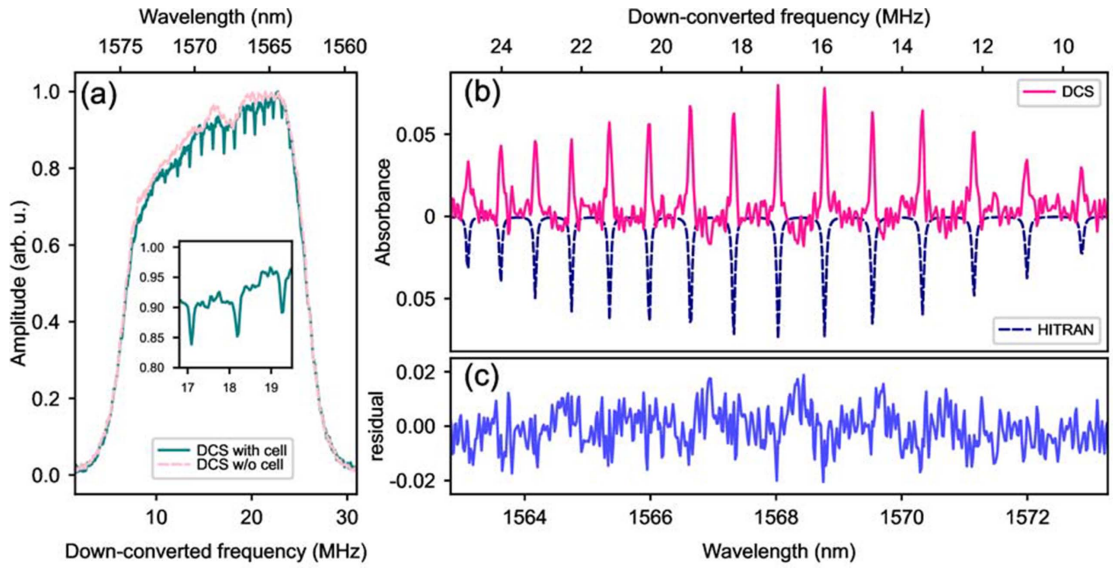

Figure 5. DC spectroscopy of CO. The difference in repetition rates of the laser is set to 1.04 kHz. (a) The down-converted RF spectrum was obtained after performing FFT of an average of 250 interferograms with CO cell (teal) and without cell (dashed pink). (b) The deep pink line shows the absorption spectrum from DC detection while the blue-dashed lines depict the HITRAN curve. The HITRAN data is calculated for a path length of 30 cm, 790 Torr and 296 K. (c) The residuals (HITRAN—DC) from (b) after fitting.

1.04 kHz and $f_{rep} = 74.74$ MHz. These 250 interferograms were averaged in the time domain after applying a phase correction algorithm from [46]. Afterward, an FFT was performed to obtain the down-converted RF spectrum (figure 5(a)). The same procedure is carried out without the cell to obtain a background spectrum, also shown in figure 5(a). Subtracting the resulting spectrum with cell from the background spectrum, we obtain the absorption spectrum of CO. To perform DC spectroscopy, one needs a reference spectrum. In our case, we used an absorption peak of CO measured by a calibrated grating-based optical spectrum analyzer (Yokogawa AQ6374). The wavelength shift for this down-converted RF spectrum to the optical domain is then carried out with the help of the reference spectrum. Afterward, the absorption spectrum is compared with the reference data from HITRAN with the same temperature, pressure, and resolution as that of DC [48]. Figure 5(b) shows the resulting absorption spectrum (deep pink) of CO after background subtraction and baseline correction of the DC system. For multiple measurements, the fitting parameters for the wavelength shift can slightly differ from environmental perturbances. However, as long as these parameters are within the uncertainty range, they will provide consistent results. The absorption lines detected by the DC system exhibit good agreement with those derived from HITRAN (blue-dashed lines), as depicted in figure 5(b). The residuals of the experiment are shown in figure 5(c). It is calculated by the difference between HITRAN and DC spectroscopic data. It is to be noted that the value of the residuals is within the noise floor of the measurement system. This shows the spectroscopic capability of this DC system even in free-running operation.

5. Conclusion and outlook

We have demonstrated a new method to build a PM Er SCDC laser based on polarization multiplexing. This simple approach leverages the fast and slow axes of the PM fiber for DC generation while using a NALM to achieve stable modelocking. The key features of our system include long-term stability, dynamic tuning in the difference in repetition rates of the laser, and the absence of sophisticated components. Our subsequent proof-of-principle measurements of CO absorption features have demonstrated the capability and robustness of our system for DC spectroscopy. Since both combs share the same gain medium and pump diode, most of the system noise is common mode, thereby enhancing mutual coherence. Compared to previous work on gain sharing [42], we increased the non-aliasing bandwidth by a factor of ~150 and the average power by a factor of 6. Our system also has the advantage of having inherent spectral overlap, unlike dual-color systems. In the work of Fellinger *et al* [32], where they use spectral subdivision, one must amplify and broaden one of the combs to achieve spectral overlap. Therefore, additional setup is required, which is not the case in our system with polarization multiplexing. Moreover, replicating this type of system is complicated and a limiting factor. Furthermore, for a mechanically shared DC system, two different gain

fibers and the same pump diode for both combs are utilized [39]. This laser is more straightforward to develop. However, since they do not share the same gain media, coherence between the two combs could decrease because of less common-mode noise. Nevertheless, in our system, the gain fiber and the pump diode are common to both combs, which are the prime components that introduce noise. Therefore, a lot of common-mode noise could lead to enhanced mutual coherence.

Moreover, having one of the end mirrors on a translational stage makes it easier to tune the difference in the repetition rates of the laser. By means of this translatable mirror, we were able to tune the Δf_{rep} from 500 Hz to 200 kHz. This plays a crucial role in the trade-off between the acquisition rate and the non-aliasing bandwidth, which becomes relevant for DC spectroscopy. Notably, the system stayed in stable DC operation for several months. We also measured the noise performance of the DC system, including both RIN and PN. Despite the construction site nearby and the disturbances, the laser demonstrated good noise behavior. Both the fast and slow axes exhibited the same PN performance, resulting in better mutual coherence. This characteristic is relevant for DC spectroscopic experiments.

The DC spectroscopic capability of this system was demonstrated as a proof-of-principle experiment by measuring the transmission curve of a CO reference cell. After data processing, including background and baseline correction, as well as a comparison to HITRAN reference data, we were able to resolve absorption peaks with an optical resolution of 3.6 GHz in a completely free-running operation. Although the noise floor of the DC system needs improvement, the residuals remain within the noise floor. Enhancement of the SNR will be addressed in future works, for instance, by using real-time data processing [24]. This proof-of-principle detection of CO and the DC scheme make this system a promising candidate for the development of compact, robust, and high-resolution spectrometers tailored for field-deployable spectroscopy.

Data availability statement

The data cannot be made publicly available upon publication because they are not available in a format that is sufficiently accessible or reusable by other researchers. The data that support the findings of this study are available upon reasonable request from the authors.

Acknowledgments

We thank Maximilian Prinz, Vito F Pecile, Felix Harfmann, Zbigniew Łaszczych, and Monika Bahl for valuable discussions. This research was funded in whole or in part by the Austrian Science Fund (FWF)[10.55776/ P33680]. For open access purposes, the author has applied a CC BY public copyright license to any author accepted manuscript version arising from this submission. The financial support by the Austrian Federal Ministry of Labour and Economy, the National Foundation for Research, Technology and Development and the Christian Doppler Research Association is gratefully acknowledged.

Jiayang Chen is a visiting student who would like to acknowledge the support from the China Scholarship Council.

Certain instruments are identified in this paper in order to specify the experimental procedure adequately. Such identification is not intended to imply recommendation or endorsement by all the authors, nor is it intended to imply that the instruments identified are necessarily the best available for the purpose.

Conflict of interest

The authors have no conflicts to disclose.

ORCID iDs

P E Collin Aldia https://orcid.org/0000-0001-7186-0030
Jiayang Chen https://orcid.org/0000-0002-8695-2082
Lukas W Perner https://orcid.org/0000-0001-8872-2072

References

[1] Diddams S A, Hollberg L and Mbele V 2007 Molecular fingerprinting with the resolved modes of a femtosecond laser frequency comb *Nature* **445** 627–30

[2] Alden C B, Ghosh S, Coburn S, Sweeney C, Karion A, Wright R, Coddington I, Prasad K and Rieker G B 2017 Methane leak detection and sizing over long distances using dual frequency comb laser spectroscopy and a bootstrap inversion technique *Atmos. Meas. Tech. Discuss.* **2017** 1–34

[3] Minoshima K and Matsumoto H 2000 High-accuracy measurement of 240-m distance in an optical tunnel by use of a compact femtosecond laser *Appl. Opt.* **39** 5512–7
[4] Rosenband T *et al* 2008 Frequency ratio of Al+ and Hg+ single-ion optical clocks; metrology at the 17th decimal place *Science* **319** 1808–12
[5] Baltuška A *et al* 2003 Attosecond control of electronic processes by intense light fields *Nature* **421** 611–5
[6] Picqué N and Hänsch T W 2019 Frequency comb spectroscopy *Nat. Photon.* **13** 146–57
[7] Coddington I, Newbury N and Swann W 2016 Dual-comb spectroscopy *Optica* **3** 414–26
[8] Shumakova V and Heckl O H 2024 A short guide to recent developments in laser-based gas phase spectroscopy, applications and tools *APL Photonics* **9** 010803
[9] Ideguchi T, Holzner S, Bernhardt B, Guelachvili G, Picqué N and Hänsch T W 2013 Coherent raman spectro-imaging with laser frequency combs *Nature* **502** 355–8
[10] Lomsadze B, Smith B C and Cundiff S T 2018 Tri-comb spectroscopy *Nat. Photon.* **12** 676–80
[11] Thorpe M J, Moll K D, Jones R J, Safdi B and Ye J 2006 Broadband cavity ringdown spectroscopy for sensitive and rapid molecular detection *Science* **311** 1595–9
[12] Rieker G B *et al* 2014 Frequency-comb-based remote sensing of greenhouse gases over kilometer air paths *Optica* **1** 290–8
[13] Bates J B 1976 Fourier transform infrared spectroscopy: the basic principles and current applications of a rapidly expanding technique are reviewed *Science* **191** 31–37
[14] Maslowski P *et al* 2016 Surpassing the path-limited resolution of fourier-transform spectrometry with frequency combs *Phys. Rev.* A **93** 021802
[15] Shirasaki M 1996 Large angular dispersion by a virtually imaged phased array and its application to a wavelength demultiplexer *Opt. Lett.* **21** 366–8
[16] Schiller S 2002 Spectrometry with frequency combs *Opt. Lett.* **27** 766–8
[17] Coddington I, Swann W C and Newbury N R 2008 Coherent multiheterodyne spectroscopy using stabilized optical frequency combs *Phys. Rev. Lett.* **100** 013902
[18] Coddington I, Swann W C, Nenadovic L and Newbury N R 2009 Rapid and precise absolute distance measurements at long range *Nat. Photon.* **3** 351–6
[19] Fellinger J *et al* 2021 Simple approach for extending the ambiguity-free range of dual-comb ranging *Opt. Lett.* **46** 3677–80
[20] Tian H, Li R, Endo T, Kato T, Asahara A, Sterczewski L A and Minoshima K 2022 Dual-comb spectroscopy using free-running mechanical sharing dual-comb fiber lasers *Appl. Phys. Lett.* **121** 211104
[21] Qin Y, Cromey B, Batjargal O and Kieu K 2021 All-fiber single-cavity dual-comb for coherent anti-stokes raman scattering spectroscopy based on spectral focusing *Opt. Lett.* **46** 146–9
[22] Truong G-W, Waxman E M, Cossel K C, Baumann E, Klose A, Giorgetta F R, Swann W C, Newbury N R and Coddington I 2016 Accurate frequency referencing for fieldable dual-comb spectroscopy *Opt. Express* **24** 30495–504
[23] Giaccari P, Deschênes J-D, Saucier P, Genest J and Tremblay P 2008 Active fourier-transform spectroscopy combining the direct rf beating of two fiber-based mode-locked lasers with a novel referencing method *Opt. Express* **16** 4347–65
[24] Ideguchi T, Poisson A, Guelachvili G, Picqué N and Hänsch T W 2014 Adaptive real-time dual-comb spectroscopy *Nat. Commun.* **5** 3375
[25] Ideguchi T, Nakamura T, Kobayashi Y and Goda K 2016 Kerr-lens mode-locked bidirectional dual-comb ring laser for broadband dual-comb spectroscopy *Optica* **3** 748–53
[26] Galtier S, Pivard C, Morville Jérôme and Rairoux P 2022 High-resolution dual comb spectroscopy using a free-running, bidirectional ring titanium sapphire laser *Opt. Express* **30** 21148–58
[27] Gu X, Wang G, Li Y, Gong H, Liang Y, Wu T, Wang J and Liu Y 2023 Polarization-multiplexed, single-cavity dual-comb fiber laser based on a birefringent crystal and a saturable absorber *Opt. Express* **31** 56–64
[28] Willenberg B, Pupeikis J, Krüger L M, Koch F, Phillips C R and Keller U 2020 Femtosecond dual-comb Yb:CaF_2 laser from a single free-running polarization-multiplexed cavity for optical sampling applications *Opt. Express* **28** 30275–88
[29] Pupeikis J, Willenberg B, Camenzind S L, Benayad A, Camy P, Phillips C R, Keller U, Fellinger J and Winkler G 2022 Spatially multiplexed single-cavity dual-comb laser *Optica* **9** 713–6
[30] Zhao X, Li T, Liu Y, Li Q and Zheng Z 2018 Polarization-multiplexed, dual-comb all-fiber mode-locked laser *Photon. Res.* **6** 853–7
[31] Sterczewski Łukasz A, Przewłoka A, Kaszub W and Sotor J 2019 Computational doppler-limited dual-comb spectroscopy with a free-running all-fiber laser *APL Photonics* **4** 116102
[32] Fellinger J, Mayer A S, Winkler G, Grosinger W, Truong G-W, Droste S, Li C, Heyl C M, Hartl I and Heckl O H 2019 Tunable dual-comb from an all-polarization-maintaining single-cavity dual-color Yb:fiber laser *Opt. Express* **27** 28062–74
[33] Fellinger J, Winkler G, Mayer A S, Steidle L R and Heckl O H 2019 Tunable dual-color operation of Yb:fiber laser via mechanical spectral subdivision *Opt. Express* **27** 5478–86
[34] Zhao X, Zheng Z, Liu L, Liu Y, Jiang Y, Yang X and Zhu J 2011 Switchable, dual-wavelength passively mode-locked ultrafast fiber laser based on a single-wall carbon nanotube modelocker and intracavity loss tuning *Opt. Express* **19** 1168–73
[35] Liao R, Song Y, Liu W, Shi H, Chai L and Hu M 2018 Dual-comb spectroscopy with a single free-running thulium-doped fiber laser *Opt. Express* **26** 11046–54
[36] Mayer A S *et al* 2020 Flexible all-pm nalm Yb:fiber laser design for frequency comb applications: operation regimes and their noise properties *Opt. Express* **28** 18946–68
[37] Kuse N, Jiang J, Lee C-C, Schibli T R and Fermann M E 2016 All polarization-maintaining er fiber-based optical frequency combs with nonlinear amplifying loop mirror *Opt. Express* **24** 3095–102
[38] Hänsel W 2018 All polarization-maintaining fiber laser architecture for robust femtosecond pulse generation *Exploring the World With the Laser: Dedicated to Theodor HäNsch on his 75th Birthday* (Springer) pp 331–40
[39] Nakajima Y, Kusumi Y and Minoshima K 2021 Mechanical sharing dual-comb fiber laser based on an all-polarization-maintaining cavity configuration *Opt. Lett.* **46** 5401–4
[40] Nakajima Y, Hata Y and Minoshima K 2019 All-polarization-maintaining, polarization-multiplexed, dual-comb fiber laser with a nonlinear amplifying loop mirror *Opt. Express* **27** 14648–56
[41] Rao B, Li M, Yang X, Yan L, Chen X, Yuan R, Zhang P and Zhang S 2022 Polarization-multiplexed dual-comb fiber laser based on an all-polarization-maintaining cavity configuration *Frontiers Phys.* **10** 1073201
[42] Iwakuni K, Takahashi A and Okubo S 2023 Noise characteristics of a polarization-duplex dual-comb fiber laser based on a single gain fiber *Res. Opt.* **12** 100476
[43] Ideguchi T 2017 Dual-comb spectroscopy *Opt. Photonics News* **28** 32–39

[44] Paschotta R 2024 Erbium-doped laser gain media RP Photonics Encyclopedia (available at: www.rp-photonics.com/erbium_doped_laser_gain_media.html)
[45] Wei Y, Li B, Wei X, Yu Y and Wong K K Y 2018 Ultrafast spectral dynamics of dual-color-soliton intracavity collision in a mode-locked fiber laser *Appl. Phys. Lett.* **112** 081104
[46] Phillips C R, Willenberg B, Nussbaum-Lapping A, Callegari F, Camenzind S L, Pupeikis J and Keller U 2023 Coherently averaged dual-comb spectroscopy with a low-noise and high-power free-running gigahertz dual-comb laser *Opt. Express* **31** 7103–19
[47] Di Domenico G, Schilt S and Thomann P 2010 Simple approach to the relation between laser frequency noise and laser line shape *Appl. Opt.* **49** 4801–7
[48] Borkov Y G, Solodov A M, Solodov A A, Petrova T M, Karlovets E V and Perevalov V I 2020 Fourier transform co spectra near 1.6 μm *J. Quant. Spectrosc. Radiat. Transfer* **253** 107064